

Characterization of the impact of network topology on the performance of single-radio wireless mesh networks

Tânia Calçada · Manuel Ricardo

Published online: 13 August 2013
© Springer Science+Business Media New York 2013

Abstract Stub Wireless Mesh Networks (WMNs) are used to extend Internet access. The use of multiple channels improves the capacity of WMN but significant challenges arise when nodes are limited to a single-radio interface to form the WMN. In particular, the assignment of mesh nodes to channels results on the creation of multiple sub-networks, one per channel, where individual capacity may depend on the sub-network topologies. This paper identifies the relevant topological characteristics of the sub-networks resultant from the channel assignment process and studies, through simulation, the impact and relative importance of those characteristics on the maximal throughput enabled by the stub WMN. The number of nodes in the gateways neighborhood and the hidden node problem in the gateways neighborhood were identified as the characteristics having the highest impact on the WMN throughput.

Keywords Channel assignment · Hidden node problem · Multi-channel · Single-radio · Topology metrics · Wireless mesh networks

1 Introduction

WMNs are emerging as a low-cost solution for broadband Internet access. A WMN node is a wireless packet switch that may accumulate the function of wireless access point.

T. Calçada (✉) · M. Ricardo
INESC TEC (formerly INESC Porto), Faculdade de Engenharia,
Universidade do Porto, Porto, Portugal
e-mail: tcalcada@fe.up.pt

M. Ricardo
e-mail: mricardo@inescporto.pt

WMN nodes are interconnected by wireless links and, together, they enable redundant paths and help increasing the network reliability.

This paper addresses the network scenario represented in Fig. 1, used to extend the access to the Internet, and it is similar to the scenario addressed in [8] and by IEEE 802.11s [14]. In this scenario, WMN nodes are expected to have two wireless cards with independent of-the-shelf radio interfaces running the standard MAC 802.11 protocol; one radio interface operates as an access point and the other is used to interconnect the node to the WMN. WMNs connect to the infrastructured wire network via special nodes acting as gateways to the Internet.

The fundamental access method of the IEEE 802.11 MAC [13] is a Distributed Coordination Function (DCF) known as Carrier Sense Multiple Access with Collision Avoidance (CSMA/CA). For a node to transmit, it first

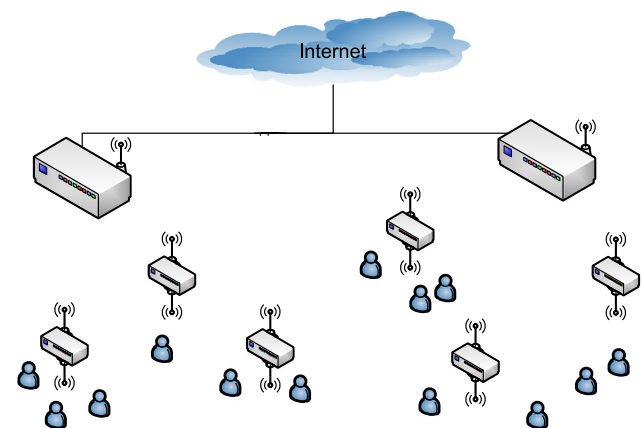


Fig. 1 WMN scenario deployed to extend Internet access, where nodes form a WMN and simultaneously serve as access points to unmodified clients. WMNs connect to the infrastructured wire network via special nodes acting as gateways to the Internet

senses the medium to determine if another node is transmitting. If the medium is not busy, the transmission proceeds; otherwise, the node defers until the end of the current transmission, where it tries to transmit the frame after a random waiting time. A refinement of the method may be used to further minimize collisions; transmitting and receiving nodes exchange short control frames, Request To Send (RTS) and Clear To Send (CTS), to determine if the medium is idle prior to data transmission.

As the number of active nodes in a wireless network increases, the number of frames transmitted by each node falls down since these nodes are sharing a wireless medium of finite capacity [12]. This problem is more critical on highly loaded scenarios, where long deferring times are introduced. Network capacity increases with the number of channels in use as shown in [19, 21].

Our work considers that WMN nodes have a single radio interface available to establish the WMN. This option may be taken due to hardware restrictions such as those reported at [28] and [27] or by economical restrictions. We assume that if two radios are available at each WMN node, one of them is used as access point to provide access to stations, leading us to a single-radio WMN.

There is significant work done in channel assignment strategies for WMNs [29], however few of these works consider single-radio WMN nodes. A survey is available in [10], where most of the approaches presented stand on dynamic channel switching [7, 31] which require dedicated MAC layer protocols and tight time synchronization between nodes. Other single-radio proposals ([30] and [33]) assign all nodes on a path to a common channel, not demanding changes on MAC layer. This assignment is considered quasi-static since it is static for long periods of time but should be changed to face significant alterations on the network topology or traffic demands.

The overall objective of most multi-radio or dynamic channel switching single-radio approaches studied in the past few years ([2, 5, 7, 11, 23, 31, 32]) was to minimize the overall network interference. This approach was triggered by the work in [12] which states that minimizing the network interference results in improving the overall network capacity. This statement is true when there are multiple radios on each node (or when they synchronously change channels) where channel assignment can avoid adjacent nodes to interfere. When a quasi-static channel is assigned to each node, adjacent links (links sharing a node) always interfere and therefore cannot be used simultaneously. In this case it is not obvious that minimizing the network interference improves the network capacity.

Works at [30] and [33] are quasi-static single-radio channel assignment proposals. The protocol presented at [30] aims to increase the network performance by reducing the load in each sub-network which is achieved by reducing the

active path length. However, it is not proved that by just reducing path length more efficient networks are obtained. The approach used in [33] increases throughput by reducing number of contending flows on a channel, which is achieved by reducing the node density on each channel. However, reducing node density makes the network less connected and more susceptible to the occurrence of collisions caused by hidden nodes; this strategy may be not satisfactory in Internet access scenarios because collisions occur more frequently when nodes in the neighborhood of intersecting nodes (e.g. gateways) are hidden from each other, despite facing less contention.

Our work aims to characterize the impact of network topology characteristics (e.g. path hop count, node density and hidden nodes) on the performance of a WMN. We consider this characterization fundamental for designing a quasi-static channel assignment algorithm for single-radio WMNs and, to the best of our knowledge, it is not available on the state-of-the art. The performance of the WMN depends of its topology characteristics [24], therefore it is important to know the relevant topology characteristics and the metrics that extract this information from the topology. For that purpose, we defined a set of experiments with 18 arbitrary channel assignment scenarios in a 6×6 lattice topology network and 8000 random scenarios. We used ns-2 simulations and, based on the results obtained, we have identified the topology characteristics that have relevant impact on the throughput of the WMN.

This work provides two main contributions:

1. Identification of simple wireless network topology metrics that are related to the performance of WMNs and can be used for deciding about channel assignment in WMNs. The metrics identified are the following: (a) mean hop count; (b) neighbor node density, which is the mean number of neighbors of a mesh node; (c) *miss ratio*, which synthesizes the number of hidden nodes on the network; (d) number of nodes in the 1st ring, which are the nodes directly connected to gateway; (e) mean number of hidden nodes on the 1st ring; (f) 1st ring *miss ratio*.
2. Evaluating and ranking the impact of topology metrics on the performance of the WMN. By decreasing order of importance, the relevant topology metrics were found to be the following: (a) the number of nodes directly connected to the gateway and the mean number of hidden nodes on links to the gateway, which are by far the most important metrics in the scenarios studied; (b) the *miss ratio* metric, which also has an high impact; (c) the mean hop count and neighbor node density, which have low impact on the network performance.

The rest of the paper is organized as follows. Section 2 characterizes network topology characteristics and derives a

set of related topology metrics. Section 3 defines the problem to be solved and describes the methodology used in our study. Sections 4 and 5 present the results of this study for a set of arbitrary and random scenarios. Section 6 concludes the paper, presents future work and identifies possible applications of our results.

2 Topology characteristics

2.1 Hop count

The MAC carrier sensing mechanism prevents simultaneous transmissions of neighbor nodes that can sense each other. In order to avoid collisions, the neighbors of both the receiver and the transmitter of a frame should be silent when the communication takes place. Consider the chain network on Fig. 2 with a carrier sense range equal to the receiving range (small solid circles around nodes) and data frames being transmitted from left to right; when Node B is transmitting a data frame to Node C, Node A and Node D should be silent, while Node E and Node F are allowed to transmit.

Nodes with network interfaces working in half duplex are either receiving or transmitting traffic. When data transverse 2 hops to reach the destination, the network throughput is reduced to 1/2 of the capacity because each frame has to be transmitted twice through the same medium. Refer to Fig. 2, considering that the Node A is the source and Node C is the flow destination. In this case, Node B can be either receiving from A or transmitting to C. If 3 hops are involved, the final data rate of the network is not expected to be more than 1/3 of the channel capacity. When the carrier sense range is the double of the receiving range, the network throughput is 1/4 of the channel capacity. For a non ideal scheduling, a throughput of 1/5 of channel data rate

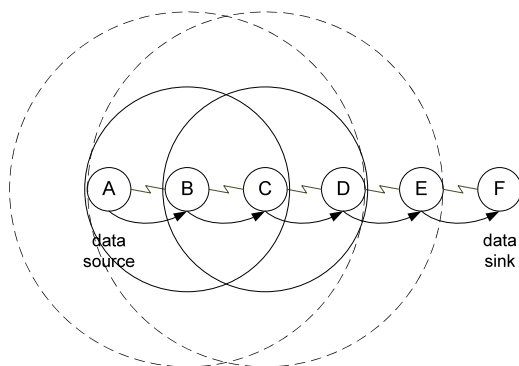


Fig. 2 Chain network topology with a single flow. A single flow is transmitted along a 6 node chain network. The *small solid lines* around nodes B and C represent the receiving range and the carrier sensing range when the latter equals the former. The *large dotted circles* represent the carrier sensing range when it is the double of the receiving range

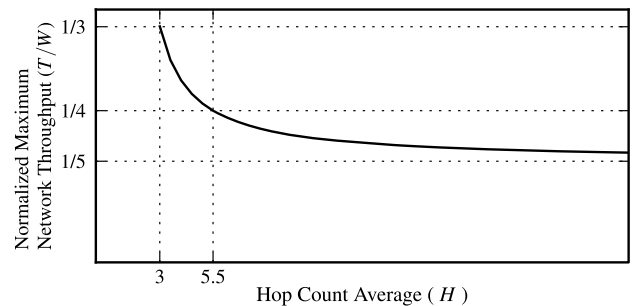
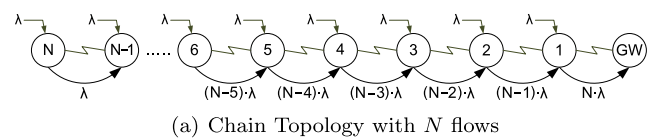
has been reported in [26] when the carrier sense range doubles the receiving range. In [22], simulation results shown that the chain network throughput is 1/7 of the single-hop throughput for this network topology.

For chain networks such as those represented in Fig. 2 it is possible to demonstrate that the length of the chain does not affect the maximum achievable throughput when a single flow is using the network; however, when several sources are used, the length of the chain influences the maximum achievable throughput.

An upper bound for the throughput of a node in a wireless chain network is given in [17]. The analysis is not limited to a specific MAC, but the result can be applied to IEEE 802.11. The concept of bottleneck collision domain is introduced there by defining it as the geographical area of the network that enables an upper bound on the amount of data that can be transmitted in the network. This concept enables the derivation of the impact the mean number of hops H has in a given network, when all nodes are sources of flows with the same packet rate of λ packet/s destined to a common sink. The mean number of hops H traversed by a packet in the network of Fig. 3(a) is given by Eq. (1), where N indicates the number of nodes in the network.

$$H = \frac{1}{N} \sum_{n=1}^N n = (N + 1)/2 \tag{1}$$

The bottleneck collision domain of the network of Fig. 3(a) is the collision domain of link 2–3 composed by links {GW–1, 1–2, 2–3, 3–4, 4–5} [17]. Each collision domain has to forward the sum of the traffic of its links. In this case, the collision domain of link 2–3 has to forward $\lambda \cdot [(N - 4) + (N - 3) + (N - 2) + (N - 1) + N] = \lambda \cdot (5N - 10)$. The collision domain cannot forward more



(b) Maximum network throughput T as a function of mean hop count H for a given channel data rate W

Fig. 3 In chain topologies all the nodes are sources of a data flow with packet rate λ pkt/s destined to the gateway GW. Considering these topologies, the maximum network throughput T tends to $W/5$

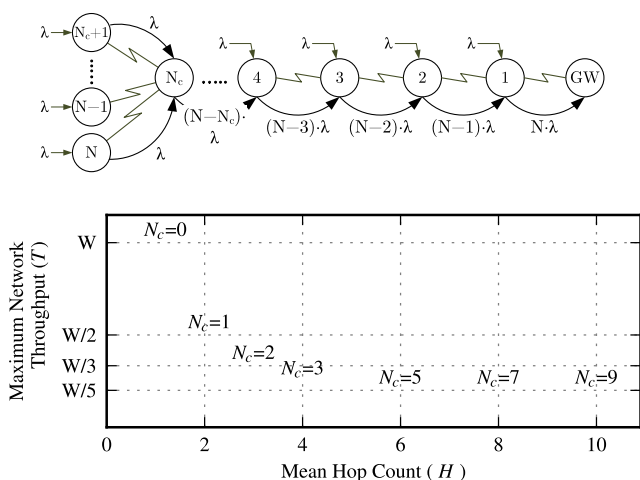


Fig. 4 Topologies combining a chain of N_c nodes and a star of $N - N_c$ nodes. The throughput of star-chain topology networks is represented as a function of the mean hop count H from each node to the gateway assuming $N = \infty$

traffic than the channel data rate W , what means that $W \geq \lambda \cdot (5N - 10)$. Therefore, the maximum throughput available for each node is $\lambda_{max} = W/(5N - 10)$ and the maximum network throughput T is given by Eq. (2), where $N = 2H - 1$ comes from Eq. (1).

$$T \leq N\lambda_{max} \leq \frac{N \cdot W}{5N - 10} = \frac{W(2H - 1)}{5(2H - 1) - 10} = \frac{W(2H - 1)}{10H - 15} \tag{2}$$

Figure 3(b) represents a plot of Eq. (2). The global throughput T decreases with the mean number of hops on a chain but it is lower bounded by $W/5$.

Let us consider now the topologies of Fig. 4, that combine a chain of N_c nodes and a star of $N - N_c$ nodes. When $N_c = 0$ the network has star topology; when $N_c = N - 1$ the network is a chain topology. All the topologies present the same number of nodes $N = 8$ but different mean hop count H . In this case, the mean hop Count H is given by Eq. (3), where the first addend refers to the N_c nodes on the chain part of the network, and the second addend refers to the $N - N_c$ nodes on the star part of the network.

$$H = \frac{\sum_{n=1}^{N_c} n + [(N - N_c) \cdot (N_c + 1)]}{N} = \frac{(N_c + 1)(N - N_c/2)}{N} \tag{3}$$

When $N_c \leq 4$, all links are on the same collision domain [17]; the traffic on this collision domain is the traffic on links on the star part of the network given by $\lambda(N - N_c)$ and the traffic on the chain part of the network given by $\lambda \sum_{n=0}^{N_c-1} (N - n)$. The collision domain cannot transport more traffic than the channel data rate W , as presented by

Eq. (4)

$$W \geq \lambda(N - N_c) + \lambda \sum_{n=0}^{N_c-1} (N - n) \geq \lambda N \frac{(N_c + 1)(N - N_c/2)}{N}, \quad N_c \leq 4 \tag{4}$$

By using H from Eq. (3) in Eq. (4) it is possible to obtain $W \geq \lambda NH$ for $N_c \leq 4$. Therefore, the maximum throughput available for each node is $\lambda_{max} = W/(NH)$ and the upper bound of network throughput $T = N\lambda_{max}$ is given by Eq. (5).

$$T \leq \frac{W}{H}, \quad N_c \leq 4 \tag{5}$$

When $N_c > 4$, the bottleneck collision domain on star-chain networks of Fig. 4 is the collision domain of link 2–3 composed by links {GW–1, 1–2, 2–3, 3–4, 4–5} [17]. Each collision domain has to forward the sum of the traffic of its links. In this case, the collision domain of link 2–3 has to forward $\lambda \cdot [(N - 4) + (N - 3) + (N - 2) + (N - 1) + N] = \lambda \cdot (5N - 10)$. The collision domain cannot forward more traffic than the channel data rate W , what means that $W \geq \lambda \cdot (5N - 10)$. Therefore, the maximum throughput available for each node is $\lambda_{max} = W/(5N - 10)$ and the upper bound of network throughput $T = N \cdot \lambda_{max}$ is given by Eq. (6).

$$T \leq \frac{WN}{5N - 10}, \quad N_c > 4 \tag{6}$$

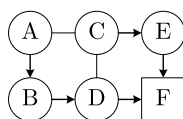
The maximum achievable throughput given by Eqs. (5) and (6) is represented in the lower part of Fig. 4 as a function of H for $N = \infty$; this graph shows that, for these topologies, the maximum achievable throughput T tends to the inverse of H . However, T does not always vary with H ; for $H \geq 5$, which corresponds to $N_c \geq 4$, T is fixed to $W/5$. Therefore, the inference of the maximum achievable throughput is not possible for a generic network by just knowing H .

2.1.1 Discussion

Two simple topologies were studied relating the mean hop count and an upper bound of the network throughput calculated as in [17]. In both examples, it was shown that when the mean hop count is not too small, i.e. $H > 6$, the influence of the mean hop count on network throughput is negligible.

In [12] the authors proved that the amount of traffic λ generated by each node that can be transmitted through the network is inversely proportional to the mean number of hops H of the network. The number of MAC transmissions generated by each flow is given by $H\lambda$. With a total number of N nodes, the total offered traffic becomes $T_n = H\lambda N$. In ideal conditions, the offered traffic has to be served by N nodes each capable of transmitting W , thus $H\lambda N \leq NW$.

Fig. 5 Sample topology used to discuss the topology metrics of a network



An upper bound of the throughput per node is $\lambda_{max} = W/H$. However, a closer upper bound can be found if constraints such as spacial concurrency were introduced.

2.2 Neighbor node density

Neighbor node density is defined as the mean number of nodes in the carrier sensing range of each node in the network. Assuming a CSMA/CA MAC, the higher the number of active nodes is in a region the less will be the throughput per node due to contention. Consider the network topology on Fig. 5 containing $N = 6$ nodes. The lines represent links between nodes; if a line is not represented between two nodes, these nodes cannot sense each other’s transmissions. Each node generates a data flow destined to Node F which is the gateway of this network. Data is transmitted through the paths defined by the links represented by lines with arrows. The neighbor node density d is calculated as the mean number of neighbors a node has. In this case we have nodes A, B, E and F with 2 neighbors, and nodes C and D with 3 neighbors, thus the neighbor node density for Fig. 5 is $d = [(4 \times 2) + (2 \times 3)]/6 \text{ nodes} = 2.33$.

The interference models presented in [12] and [3] capture the interference between a pair of links in a wireless network. Interference is caused by active nodes on the vicinity of both the sender and receiver of a link. The real behavior of interference in 802.11 DCF is captured in [3]. The physical and protocol models of [12] are referred in relevant studies of multichannel in WMN such as [7, 15, 19–21, 31]. In these models the throughput λ obtainable by a node is shown to decrease with the increase of the neighbor node density and given by $\lambda = \Theta(W/(\sqrt{n \log n}))$ [12] where W is the channel capacity and n is the number of nodes in the network, supposing that the n nodes are located in an area of 1 m^2 .

Consider the topologies of Fig. 6, all of them containing $N = 12$ nodes. The lines represent links between nodes; if a line is not represented between two nodes, these nodes cannot sense each other’s transmissions. Each node generates a data flow of $\lambda \text{ packet/s}$ destined to the gateway. Data is transmitted through the paths defined by the links represented by lines with arrows. Paths are the same on all topologies, therefore the mean hop count is $H = 2.5$ for the 9 topologies presented. The label of a link indicates the amount of traffic transported by that link.

The neighbor node density d is calculated as the mean number of neighbors a node has in the network. Each topology presents a different neighbor set for each node by adding new links to the base network topology of Fig. 6(a), thus originating different node densities.

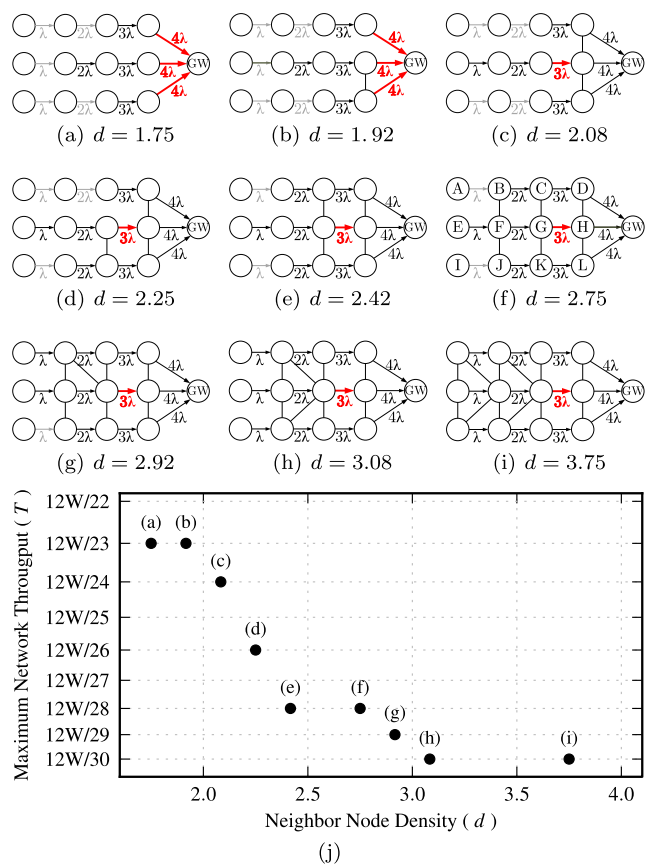


Fig. 6 Topologies with $N = 12$ nodes, mean hop count $H = 2.5$ and variable neighbor node density d are used to study the impact of neighbor node density on the network throughput. Nodes that can sense each other have a *line* between them. Nodes generate data flows of $\lambda \text{ packet/s}$ to the gateway through paths represented with *arrows* which have labels indicating the amount of transported traffic. *Stronger lines* indicates the bottleneck collision domains calculated as in [17]. A throughput *upper bound* T is plotted as a function of d showing that the inference of the T is not possible for a generic network by just knowing d

The maximum achievable throughput for these scenarios is calculated according to the model presented in [17] described earlier. The link found as the bottleneck collision domain of each topology is represented by a red strong line and the links not belonging to that collision domain are represented in gray. For instance, the bottleneck collision domain of the network on Fig. 6(f) is the collision domain of the link G–H composed by links {D–GW, H–GW, L–GW, C–D, G–H, K–L, B–C, F–G, J–K, E–F} [17]. This collision domain has to forward the sum of the traffic of its links which is $(4 + 4 + 4 + 3 + 3 + 3 + 2 + 2 + 2 + 1)\lambda = 28\lambda$. The collision domain cannot forward more traffic than the channel data rate W what implies that $28\lambda \leq W$. Therefore, the maximum throughput available to each node is $\lambda_{max} = W/28$ and the maximum network throughput is $T = N\lambda_{max} = 12W/28$, considering that $N = 12$.

The maximum achievable throughputs of topologies of Fig. 6(a) to Fig. 6(i) are plotted in Fig. 6(j) as a function of the calculated neighbor node density d . This graph shows that, for these topologies, the maximum achievable throughput T tends to be the inverse of d . However, T does not always vary with d . As shown by these topologies, in general is difficult to infer maximum achievable throughput by just knowing the neighbor node density d .

In [20], Kuo et al. prove that the throughput of a node λ is asymptotically defined as a function $f(d)$ of node density d given by Eq. (7), where c is a constant.

$$\lambda = \Theta(f(d)), \quad f(d) = \frac{1 - (d^{-1}e^{-d/c})}{d} \quad (7)$$

Authors in [20] argue that $f(d)$ is a trade-off between hop progress on the numerator and contention on the denominator. The numerator $1 - (d^{-1}e^{-d/c})$ shows that the throughput increases with the neighbor node density; when a node has a large number of neighbors, the probability that the next node on the multi-hop path is closer to the destination increases, and so does the hop progress. As a result, a large neighbor node density d leads to a smaller path hop count for each flow, which in turn reduces the traffic to be relayed by the network. The denominator shows that a large neighbor node density also introduces more contentions in the access to the wireless channel by the nodes in the receiving range. When d is small, the hop progress is more important than the contention effect; when d grows, the contention dominates. The study in [20] does not consider collisions caused by hidden nodes nor simultaneous transmissions both highly related with neighbor node density. The works reported in [1, 15, 36] address these problems. Packet collisions due to simultaneous transmissions are expected to increase with the increase of neighbor node density since it is more likely that two or more nodes of a neighborhood transmit at the same time slot. However, collisions due to hidden nodes can decrease when the neighbor node density increases since the number of hidden nodes can also decrease, what implies that for some topologies the throughput can increase when neighbor node density is high, as shown for the networks we study in our paper.

2.3 Hidden nodes

The hidden node problem is partially solved by the RTS/CTS mechanism of IEEE 802.11 on wireless local area networks. However in multi-hop networks it is proved [35] that hidden mesh nodes cause severe problems on network performance even when the RTS/CTS mechanism is used, since it does not solve the mesh hidden node problem and it increases the network overhead, leading to performance degradation.

For a given topology, the mean number of hidden nodes can be measured by averaging the number of hidden nodes

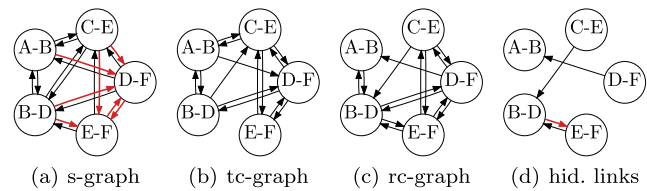


Fig. 7 In the topology of Fig. 5, (a) is the s-graph, (b) is the tc-graph, (c) is the rc-graph, and (d) represents the hidden links. The 1st ring s-graph and 1st ring hidden links are respectively the sub-set of s-graph and hidden links represented as *thicker lines (red)* (Color figure online)

of each active link in the network. The number of hidden nodes of a link is the number of neighbors of the link's receiver that are not neighbors of the link's transmitter. For instance, on Fig. 5 there are 5 active links, which are the links used to transmit data, represented by arrows. Node D is hidden from link A–B, C and F are hidden from B–D, F is hidden from C–E, E is hidden from D–F, and D is hidden from E–F. The mean number of hidden nodes of the topology of Fig. 5 is $(1 + 2 + 1 + 1 + 1)/5 = 1.2$ nodes.

Attempts to analytically characterize the impact of hidden nodes on multi-hop networks are described in [1, 6, 15]. In [6], authors derive the number of hidden nodes of a link considering the length of the link, but the relationship between the number of hidden nodes and throughput is not analyzed.

In [15], the authors introduce the *miss ratio* metric which is a global measure of the severity of the hidden nodes in the overall network. To describe the *miss ratio* metric, the authors first define a set of graphs that capture the physical interferences and the carrier sensing constraints between links in a network: s-graph, tc-graph, and rc-graph. In these graphs a vertex represents a wireless link. The s-graph can be used to capture the physical interference constraints graphically; an s-graph edge between vertex 1 and vertex 2 indicates that, in order to prevent future collisions, link 1 (node T_1 to node R_1) must be capable of forewarning link 2 (node T_2 to node R_2) not to transmit after link 1 initiates a transmission. The tc-graph models the transmitter-side carrier sensing; an tc-graph edge between vertex 1 and vertex 2 means that link 1 can and will forewarn link 2 not to transmit when link 1 is transmitting. The rc-graph models the receiver-side carrier-sensing constraints; an rc-graph edge between vertex 1 and vertex 2 indicates that R_2 will ignore T_2 transmission when the R_2 already senses a transmission on link 1. For the network of Fig. 5, s-graph, tc-graph and rc-graph are presented in Figs. 7(a), 7(b), and 7(c)

Using the graphs described above it is possible to obtain the hidden links on the network by $\overline{TC} \cap (S \cup RC)$ where S , TC , and RC are respectively the set of edges on s-graph, tc-graph, and rc-graph, and \overline{TC} represents the set of edges that are not on the tc-graph. The number of hidden links is given by $N_{HN} = |\overline{TC} \cap (S \cup RC)|$. If a tc-edge does not

exist from link 1 to link 2, the transmission of link 1 will not be sensed by T_2 . But if a rc-edge or a s-edge exists between link 1 and link 2, it indicates that either R_2 will ignore T_2 when R_2 senses a transmission on link 1 (rc-edge), or that there is physical interference from link 1 to link 2 (s-edge). In both cases, T_2 will interpret it as a collision and we can say that link 1 is hidden from link 2. The hidden links of Fig. 5 are represented in Fig. 7(d). The *miss ratio* metric is then the ratio between the number of hidden links N_{HN} and the number of edges belonging to rc-graph or s-graph, as given by Eq. (8).

$$miss\ ratio = \frac{N_{HN}}{|S \cup RC|} \tag{8}$$

When $TC = \{S \cup RC\}$ there are no hidden links N_{HN} and *miss ratio* = 0, which is the ideal value to avoid collisions on a network. In [15], the authors do not relate *miss ratio* with the network throughput. For the network on Fig. 5, $\{S \cup RC\} = \{S\}$ and $|S| = 18$, thus *miss ratio* = $4/18 = 0.22$.

In [1], the authors model the per-hop throughput T_h as a function of network parameters such as the communication sense range R , the number of nodes D per m^2 , the expected duration of frames transmission, the propagation delay, the duration of an idle slot, the minimum MAC backoff window size, and the MAC retry limit. In [1] is also shown that the number of collisions caused by hidden nodes is higher than the number of collisions caused by simultaneous transmissions; this analysis is based on graphs that plot the probability of collision caused by simultaneous transmission p_{cx} , the probability of collisions caused by hidden nodes p_{ch} and the probability of total collisions p as a function of R for a fixed number of D nodes per m^2 .

R and D enable to derive the neighbor node density as $d = \pi R^2 D$ and it is possible do plot the probability of collisions as a function of d , as shown in the left hand graph of Fig. 8. These plots show that the probability of collisions increase with the increase of the neighbor node density d . However the probability of collisions caused by hidden nodes p_{ch} does not increase continuously with d ; when there are more neighbors around a node, the neighbors of the node's neighbors are all inside the communication range of each other reducing the occurrence of hidden nodes. On the other hand, the probability of collision caused by simultaneous transmission always increase with the increase of node density; when the number of nodes in the neighborhood of a node increases it is more likely that two or more nodes start transmitting simultaneously. In [1] is also provided a graph representing the per-hop throughput T_h as a function of the communication range R . Using this graph and that relating the probabilities of collision and R , it is possible to plot the per-hop throughput T_h as a function of the probabilities of collision p , p_{ch} and p_{cx} shown in the right hand side of Fig. 8. This graph shows that the per-hop throughput is very

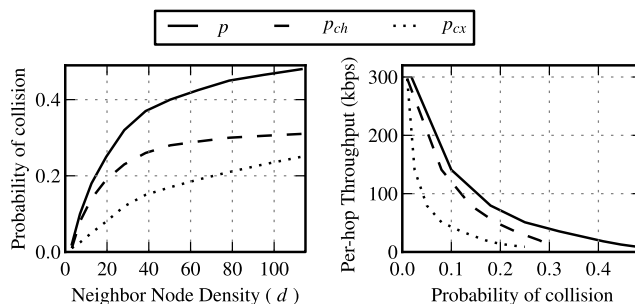


Fig. 8 The probability of collision caused by simultaneous transmission p_{cx} , the probability of collisions caused by hidden nodes p_{ch} and the probability of total collisions p can be related with the node density d . Using the results presented in [1] the per-hop throughput T_h can be related with the probability of collision

influenced by the probability of collisions. In particular, the probability of collisions caused by hidden nodes p_{ch} has a high correlation with the throughput T_h .

2.4 GW position and topology of GW neighborhood

In a scenario where a WMN is used to extend Internet access, we foresee that gateway position has a great impact on performance of the wireless network. A gateway on a central position leads to short paths; a gateway deployed on the edge of the WMN may lead to a small number of contending nodes around it.

In order to characterize the position of the gateway we introduce the concept of ring. The n th ring is the set of nodes located n hops away from the gateway [9]. The 1st ring seems to be of particular interest, since its nodes share the bottleneck of the network, which is the wireless channel around the gateway. The neighbor node density around the gateway can be measured by simply checking the size of the 1st ring, which is the number of nodes at one hop distance to and from the gateway. The hidden nodes of the 1st ring can either be measured by calculating the mean number of hidden nodes of 1st ring links or by calculating the *miss ratio* of the 1st ring. The 1st ring links are the links between the 1st ring nodes and the gateway.

The 1st ring *miss ratio* is calculated using S_{R1} , TC_{R1} and RC_{R1} which are respectively the set of edges on s-graph, tc-graph and rc-graph which affect the gateway, as given by Eq. (9)

$$miss\ ratio_{R1} = \frac{N_{HN_{R1}}}{|S_{R1} \cup RC_{R1}|} \tag{9}$$

where $N_{HN_{R1}} = |\overline{TC_{R1}} \cap (S_{R1} \cup RC_{R1})|$ is the number of links hidden from 1st ring links. For the network on Fig. 5, the S_{R1} and HN_{R1} are the bold red edges in Figs. 7(a) and 7(d), $|S_{R1} \cup RC_{R1}| = 7$ and $|HN_{R1}| = 1$ thus $miss\ ratio_{R1} = 1/7 = 0.14$.

2.5 Discussion

This section characterizes the relevant topology characteristics of WMNs that can be related with the network throughput. Metrics for these characteristics are provided. In what concerns mean hop count and neighbor node density, we conclude that it is not possible to predict the maximum network throughput by just using these metrics; nevertheless, there exists an inverse relation between network throughput and mean hop count, as well as between throughput and neighbor node density. We derived two metrics to measure the hidden nodes on a network: the mean number of hidden nodes, and the *miss ratio*. Regarding the gateway neighborhood also treated as 1st ring, the relevant metrics are 1st ring size, the 1st ring *miss ratio*, and 1st ring mean number of hidden nodes.

3 Problem statement and methodology

Using multiple wireless channels in WMNs is proven [19, 21] to improve the network capacity if an appropriate channel assignment policy is used. In a single-radio WMNs, the goal of a quasi-static channel assignment algorithm is to determine in which channel each node should be working on. We recall that we assume that a single radio mesh node is a node that can use a single network interface and a single channel at a time for communicating with the other mesh nodes. Every time a mesh node is assigned to a new channel, the topology of the network changes.

We argue that the network throughput can be optimized by controlling the network topology characteristics. As seen, relevant topology metrics are the mean hop count, the neighbor node density, the mean number of hidden nodes, the *miss ratio*, the size of the 1st ring, the mean number of hidden nodes on the 1st ring, and the *miss ratio* on the 1st ring. These metrics change when a node is assigned to another channel. In this work, we aim to estimate the impact each metric has on the network throughput and rank these metrics. This knowledge can be used in future work to decide the channel a mesh node shall be assigned to.

3.1 Simulation setup

We estimate the impact of the topology of a network on its performance, by means of extensive simulation analysis. Firstly we defined a lattice topology and simulated 18 dual-channel arbitrary deployments. Secondly, and in order to generalize these results, simulations were carried out for 8000 randomly generated scenarios.

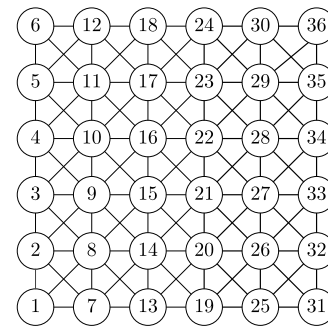


Fig. 9 6×6 lattice used to study the impact of topology characteristics on the network throughput

3.1.1 Arbitrary scenarios over a lattice topology

The 18 arbitrary channel assignment scenarios were applied to a 36 node network displaced in a 6×6 lattice topology disposed in an area of $1000 \text{ m} \times 1000 \text{ m}$, as represented on Fig. 9. The number inside a circle identifies the node. The lines represent wireless link layer connectivity; horizontal and vertical links (e.g. 1–2 or 1–7) measure 176 m and diagonal links (e.g. 1–8) measure 249 m. On figures of Sect. 4 (Fig. 11 to Fig. 21), the squares represent the gateways that have a wired connection to the Internet. Dark circles in these figures represent nodes configured on a channel, and light circles represent nodes on an orthogonal channel; these two networks are interconnected through their gateways.

The two channel assignment schemes A1 and A2 represented in Fig. 11, along with a single channel scenario (A-SCh), were used as the base scenarios to study the impact of the topology characteristics on network throughput. Scenarios B1 and B2 of Fig. 17, based on A1 and A2 but with fewer nodes, were simulated to study the effect of hop count. Scenarios C1, C2 and C-SCh of Fig. 18, based on A1 and A2 with larger carrier sensing range, were used to study the neighbor node density. Scenarios D1, D2 and D-SCh of Fig. 19, based on A1, A2 and A-SCh with gateways positioned on the center of the network, were used to understand the impact of the gateways position. Scenarios E1, E2, E3 and E4 of Fig. 20 and Scenarios A3, A4 and A5 of Fig. 21 were used to study the impact of the gateway neighborhood in terms of neighbor node density and hidden nodes.

3.1.2 Random scenarios

4000 random network topologies were also created using a TCL script added to ns-2. Each network topology has 36 nodes spread randomly in an area of $1000 \text{ m} \times 1000 \text{ m}$. The x and y coordinates of each node are random uniform variables in the interval $[0, 1000]$. Each network topology was generated randomly with the restriction that the resultant network graph should be connected, that is, every node in the network has multi-hop connectivity to all other nodes.

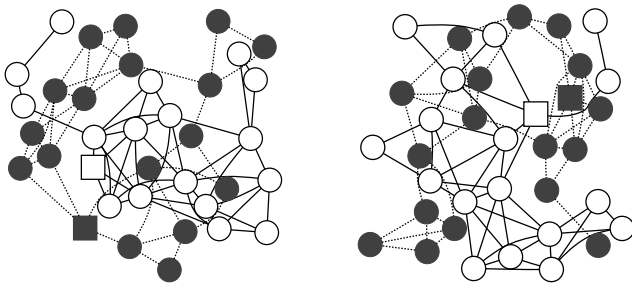


Fig. 10 Examples of random network topologies

Table 1 Parameter values used in ns-2.29 simulations

| Parameter | Value |
|-----------------------------|----------------------------|
| Propagation Model | Two ray ground |
| Channel data rate | 11 Mbit/s |
| Receiving Threshold | -70.2 dBm, 350 m |
| Node distance | 176 m |
| Main flow packet size | 1500 bytes |
| RTS/CTS | ON |
| Max. retransmission retries | 7 |
| Routing protocol | HWMP |
| Flow source type | Poisson (UDP) |
| WarmUp flow packet size | 256 byte |
| WarmUp flow data rate | 10 packet/s |
| Simulation runs | 10 (arbitrary), 3 (random) |

Two nodes from the 36 generated were randomly selected to be gateways and they operate on different radio channels.

Two different channel assignment scenarios were generated for each topology guaranteeing multi-hop connection from each node to one gateway and that the number of nodes in each channel is 18. In the first assignment, a random channel was assigned to each node. In the second channel assignment, the channel with a gateway closer in terms of hop count was assigned to each node; if both gateways were at the same distance, then the channel was selected randomly. Fig. 10 represents 2 instances of the generated networks; the lines between nodes represent wireless connectivity between them.

3.1.3 Simulator parameters

The parameters used in simulation are presented on Table 1. The simulation tool ns-2 was used with two-ray propagation model in the physical layer, and MAC DCF 802.11 in the link layer. The Hybrid Wireless Mesh Protocol (HWMP) [14] was used to establish routes since it is defined in the IEEE standard to WMNs [4]. RTS/CTS handshake was also used and the CStresh was configured to guarantee a carrier sensing range of 350 m.

3.1.4 Traffic flows

Each node generates a UDP flow towards the gateway, so 17 flows were simulated on each channel on all scenarios except the single channel scenario with 34 flows on a single channel, and Scenarios B1 and B2 which have 13 flows on each channel. A set of simulations were carried out. In each simulation all flows generated the same bit rate. Flow's bit rates from 10 kbit/s to 7.5 Mbit/s were used on arbitrary scenarios and 1 Mbit/s on the random scenarios. Flow packets are generated by a Poisson process without bursts, characterized by exponentially distributed inter-arrival times. Poisson process was selected to avoid simultaneity problems caused by other simpler approaches such as CBR. All flows are configured with similar parameters, which are fixed for each simulation; each simulation was run with 10 different seeds in the case of arbitrary scenarios and 3 different seeds in the case of random scenarios.

3.2 Duration and warm up period

Simulations run for 60 seconds, what may imply the generation of 37500 packets. During the first 3 seconds there are no data flows; this period is used to allow the HWMP routing protocol to execute the proactive tree building functionality; in this phase a route to one of the gateways is added to each node as described in the proactive Path Request (PREQ) mechanism [14]. The expiration period of routes and routing messages are set to be larger than the simulation run. This option avoids the exchange of routing messages during the main flows simulation which cause avoidable overhead and also avoids the hop count shift problem described in [34].

Between second 3 and second 4 the warm up flow takes place between each node and the gateway; this flow enables the ARP tables of each node to be filled. On second 5, the main flows start and go on until second 50. The last 10 seconds of each simulation are used to enable packets to be dequeued.

3.3 Unfairness, congestion and queuing model

Preliminary experiences with the topologies of Fig. 11 showed that the simulated scenarios exhibited serious fairness problems; for medium to high loads, only the nodes directly connected to the gateway could transmit their packets to the destination. This problem occurred because the queue of each node started to be filled by packets originated by the node's flow, and the packets received by downstream neighbors were dropped because there were no available buffers on the queue. This is a well identified and solved problem in the literature, as described in [18] and then in [25]. In our study a solution based on [25] was used where each node shares evenly the available queue among all the flows that

are being forwarded by a node, including the node's flow. In practice, a different queue was created for each flow and these queues were served by a single server using a round robin strategy. Using this approach we could guarantee that all flows have the same chance to transmit their packets at each hop of the path and we could focus on the main objective of the study which consists in analyzing the impact of topology characteristics on the network throughput.

3.4 Queue size

The queue size used in this study was 50 packets. So a node forwarding $N - 1$ flows plus its own generated flow, is able to accommodate $N \times 50$ packets. The N queues are, as said, served in round robin. In order to guarantee that these values do not affect the simulation results, we carried out simulations with smaller queue size (3 packets) and with infinite queues (200000 packets); results obtained showed that the queue size does not affect the network throughput.

3.5 Measure network topology and performance

To calculate the network topology and performance metrics on arbitrary scenarios, the two sub-networks resultant from the channel assignment are treated as a single network. The metrics aggregate the performance and the topology characteristics of all nodes in the network, independently of the channel the node is configured in. In the case of the random scenarios, two sub-networks resultant from the channel assignment are treated separately. Metrics were calculated by analyzing the trace files generated by ns-2 using python scripts and the graphs presented in Sect. 4 were created using matplotlib python library.

The performance metrics considered are the per-hop throughput and the end-to-end throughput. The per-hop throughput is defined as the mean bit rate of each data link in the network and is calculated as the total number of MAC frames successfully transmitted on the links of the network divided by the number of active links on the network which is 34 in these scenarios; non acknowledged frames are not considered. The end-to-end throughput of the network is defined as the sum of the bit rate received by the two gateways, divided by the number of sources of the network which is 34, except for Scenarios B1 and B2.

4 Arbitrary scenarios results

4.1 Basic scenarios

Two channel assignment schemes were applied to the 36 node lattice network represented in Fig. 9. The resulting networks are represented in Scenario A1 and Scenario A2

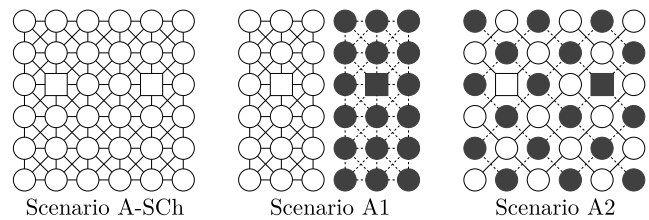


Fig. 11 The channel assignment scheme used in A1 minimizes the number of hops to the gateway. The scheme used in A2 aims to reduce the number of contending neighbors. In the single channel scheme, A-SCh, the two gateways and the rest of the nodes are on the same channel

of Fig. 11 where dark circles represent nodes configured on a channel, and light circles represent nodes on an orthogonal channel, forming two networks connected through their gateways. While the channel assignment scheme used in Scenario A1 minimizes the number of hops, the scheme used in Scenario A2 aims to reduce the neighbor node density.

Figure 12 shows the throughput and topology characteristics of the two scenarios represented in Fig. 11, and compares it with a third scenario (Scenario A-SCh) where all nodes and gateways of Fig. 9 work in a common channel. Figure 12(a) presents the per-hop throughput. For each source node debit, Fig. 12(b) presents the mean of end-to-end throughput and the 90 % confidence interval calculated using the results of the 10 simulations runs. Topology characteristics of these scenarios are presented on Fig. 12(c), and they were calculated as explained on Sect. 2; the 90 % confidence intervals of the topology metrics are also shown and indicate that the values shown are very accurate. The results on Fig. 12 are compared with results from simulations with variants of Scenarios A1 and A2 and discussed in the following sections.

4.2 Impact of traffic conditions

4.2.1 Low load traffic conditions

Low load traffic conditions are assumed when each source generates less than 120 kbit/s. In these conditions every channel assignment scheme, including the single channel, presents the same end-to-end throughput results. In low load traffic conditions, all the packets are delivered to the destination without noticeable losses, independently of the scenario used; Fig. 12(b) proves this by showing that for debits below 120 kbit/s, the end-to-end throughput is equal to the source debits. The per-hop throughput graph of Fig. 12(a) shows that the number of MAC transmissions in these conditions correspond to the number of packets received by the gateways multiplied by the number of hops of the paths followed by packets whose values are shown in Fig. 12(c).

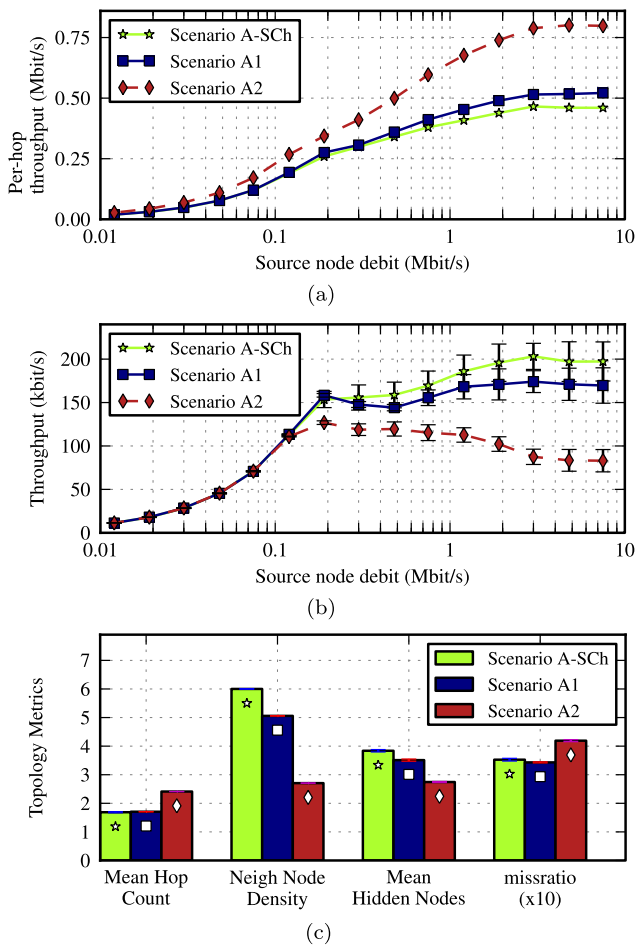


Fig. 12 (a) per-hop throughput (b) end-to-end throughput and (c) topology metrics of two dual-channel and one single channel assignment schemes presented on Fig. 11. The 90 % confidence intervals of the throughputs and topology metrics are also shown

The mean path length in Scenario A1 and in single channel scenario is 1.7, while Scenario A2 has a mean path length of 2.41. When the throughput is 120 kbit/s, which occurs when the individual source debit is 120 kbit/s, the amount of data generated by each flow along its path is $1.7 \times 120 \text{ kbit/s} = 200 \text{ kbit/s}$ in the case of Scenario A1, and $2.41 \times 120 \text{ kbit/s} = 290 \text{ kbit/s}$ for Scenario A2.

4.2.2 High traffic load conditions

When the traffic load is higher than 120 kbit/s, the end-to-end throughput starts growing slowly, in opposition to the linear growing for low loads. The networks start to lose packets and the differences of performance between the topologies start to be evident. When each individual source generates more than 3 Mbit/s, the end-to-end throughput stops growing indicating that the network is near its saturation point.

IEEE 802.11's theoretical data rate for each gateway is 11 Mbit/s, but more than 50 % [16] of it is used in overhead,

leaving 5.5 Mbit/s per gateway available to transmit packets from 34 flows. The maximum mean data rate for each flow is $5.5 \text{ Mbit/s} \times 2 \text{ gateways} / 34 \text{ nodes} = 323 \text{ kbit/s}$. Considering that each frame is forwarded through multiple hops until it reaches the gateway, the maximum achievable end-to-end throughput is even lower. Therefore, it is expectable that a considerable amount of frames are lost when the sources debit is above 0.3 Mbit/s.

4.3 End-to-end and per-hop throughputs

Figure 12(b) shows that Scenario A2 has a maximum end-to-end throughput of 127 kbit/s for the offered load of 190 kbit/s, what suggests the existence of an optimum offered load; the existence of an optimum offered load was also reported in [26] and [22]. For Scenario A1, the end-to-end throughput increases even when it starts to lose significant amounts of data (when each node source debit is higher than 300 kbit/s), and it continues to grow with increasing amounts of offered load until it reaches a saturation value of 170 kbit/s. The inefficiency of Scenario A2 for high loads is caused by hidden nodes which cause collisions. Despite the mean number of hidden nodes in Scenario A2 being lower than in the other scenarios, as shown by Fig. 12(c), the neighbor node density is also lower indicating that most of the neighbors are hidden from each other, as revealed by the *miss ratio* of Scenario A2, which is higher than in Scenario A1.

The per-hop throughput shown in Fig. 12(a) increases with the offered load until reaches the saturation values of 520 kbit/s, 800 kbit/s and 460 kbit/s respectively for Scenarios A1, A2 and A-SCh. Scenario A2 presents the highest per-hop throughput. There are two reasons for that: (1) the large value of the mean hop count of Scenario A2 observed on Fig. 12(c); (2) the low neighbor node density on the topology of Scenario A2.

4.4 Node density impact on per-hop throughput

The per-hop throughput can be easily correlated with the neighbor average for Scenarios A1 and A2 on Fig. 11. High node density results on low number of frames successfully delivered to the MAC receivers as also shown in Fig. 6. However, Scenario A2 has high per-hop throughput but low end-to-end throughput which represents the amount of packets actually delivered to the final destination. This apparent contradiction indicates that a substantial part of the frames are lost before reaching the final destination. It is expectable that frames are lost when debits are higher than 0.3 Mbit/s since all flows are destined to the gateway which is the network bottleneck.

Figure 13 shows the number of successful MAC transmissions when each node generates a traffic flow of 3 Mbit/s.

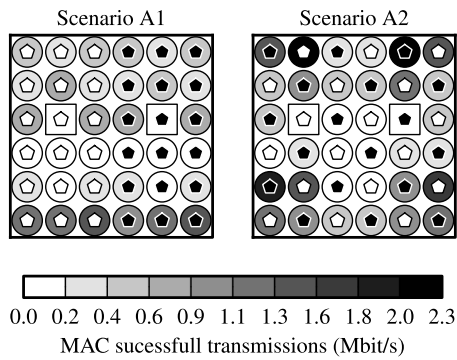


Fig. 13 Amount of data transmissions on the networks of scenarios of Fig. 11 when each node is generating a flow of 3 Mbit/s to a destination on the Internet. The *white* and *black centers* of each node represent the gateway used to forward the packets to the Internet. The *face color* of a node represents the amount of data frames that were successfully sent by that node

This load corresponds to the saturation point of Fig. 12(a). Nodes on the boundary of the network tend to acquire the channel and transmit much more packets than the other nodes on the path towards the gateway. The boundary nodes on both scenarios have few contending neighbors and the CSMA nature of IEEE 802.11 MAC protocol allows them to get the opportunity to transmit more often than subsequent nodes on the path to the gateways which have more contending neighbors. Border nodes transmit more MAC frames than interior nodes despite interior nodes have more frames to transmit, because they have to transmit their own frames and forward the frames coming from downstream neighbors. This effect makes the network inefficient because the packets that were transmitted in the first hops are then dropped near the gateway. Border nodes transmit more MAC frames on Scenario A2 than in Scenario A1 because Scenario A2 has an higher difference between the number of neighbors on border and interior nodes. This is why Scenario A2 is more inefficient than Scenario A1, what confirms the results on Fig. 12(b).

4.5 Analysis of generated packets

In our scenarios, the sources generate more packets than those that can be transported by the network. There are four possible destinies for a generated packet: (1) the packet is dropped by the source node because its queue is full; (2) the packet is dropped in an intermediate node because that queue is full if the medium around is congested; (3) the packet is dropped because the maximum number of retries defined by the IEEE 802.11 MAC is exceeded; (4) the packet succeeds if it reaches the gateway. Figure 14 quantifies these destinies for Scenario A1 and Scenario A2 of Fig. 11.

The graphs on Fig. 14 confirm the results in Fig. 12(b) showing that Scenario A1 has a higher end-to-end throughput than Scenario A2, represented in Fig. 14 by the bottom

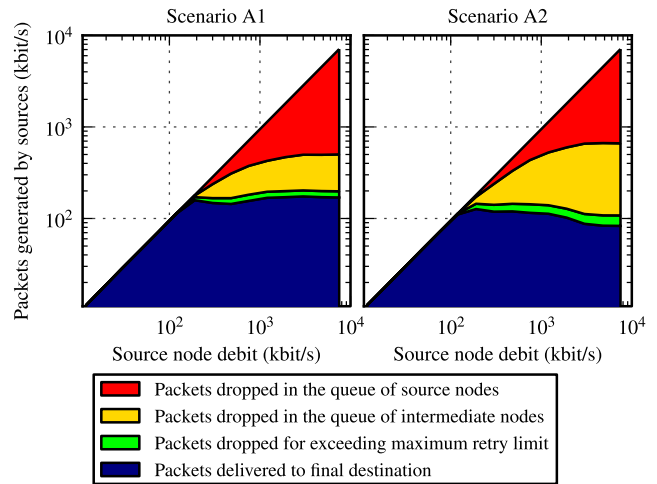


Fig. 14 Packets generated by sources (1) dropped in the queue by source nodes, (2) dropped in the queue by intermediate nodes, (3) dropped after exceeding the maximum retransmission retries limit, or (4) delivered to the final destination

layer of the curve in dark blue. The number of drops caused by exceeding the maximum retransmission retries, represented by the second layer in light green of graphs of Fig. 14, shows that the amount of collisions in Scenario A1 is lower than in Scenario A2. The number of packets dropped due to an excessive number of retries is a little fraction of the number of retransmissions.

While the nodes are retransmitting a packet multiple times due to collisions, the other packets are buffered in the queues waiting for their opportunity to be transmitted. This will cause the queue to increase and causes the drop of new packet arriving. These losses are represented in Fig. 14 by the third and fourth layers in light yellow and dark red; the combined value of drops in the queues are higher in Scenario A2 due to the amount of time that nodes in this scenario spend on retransmissions, due to collisions.

Despite the total number of drops in the queues of Scenario A2 is higher than in Scenario A1, the number of these drops that occurred in the source nodes is higher on Scenario A1. This confirms the results in Fig. 13, which show that nodes on border nodes transmit more MAC frames on Scenario A2 than in Scenario A1.

Scenario A2 shows more drops in the queues of intermediate nodes than Scenario A1, what is explained by the large number of successful transmissions by border nodes of Scenario A2. These packets are delivered to intermediate nodes which have neighbor node density higher than border nodes so the contention in the later causes packets to be buffered for more time and leads to packet drops in these queues. The asymmetry between the number of neighbors of border and interior nodes is higher in Scenario A2 than in Scenario A1.

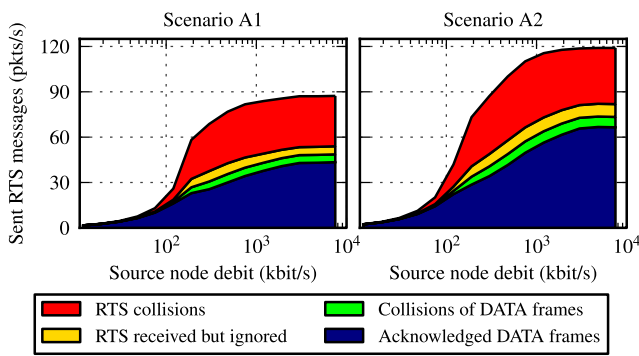


Fig. 15 After a RTS message is sent, the following may happen (1) RTS is not received, (2) RTS is successfully received but the receiver does not answer with CTS, (3) RTS is followed by a CTS and then a data frame is sent which is not received, or (4) the RTS/CTS and the DATA/ACK pairs are successfully exchanged

4.6 Analysis of collisions

The packet losses caused by exceeding the MAC retransmission retries in Scenario A2, observed in Fig. 14, indicates that this scenario has a larger amount of collisions than Scenario A1. In order to better understand the causes and impact of collisions on the network performance, the number tentatives for transmitting data frames were studied for both scenarios; result are presented in Fig. 15. For that purpose we characterize the number of RTS messages sent by nodes. After an RTS message is sent, the following may happen: (1) RTS is not received; (2) RTS is successfully received but the receiver does not answer with CTS because it senses that some other node is using the medium; (3) RTS is followed by a CTS and then a data frame is sent which is not received; or (4) the RTS/CTS and the DATA/ACK pairs are successfully exchanged.

The number of tentatives for transmitting frames, shown in Fig. 15 by the total number of RTS messages sent, is higher for Scenario A2 than for Scenario A1; this is explained, as discussed above, by the higher mean hop count and lower average number of neighbors of Scenario A2 when compared with Scenario A1. The number of RTS collisions represented by the first (top) layer in dark red of Fig. 15 is higher on Scenario A2; this can be explained by the higher *miss ratio* of Scenario A2.

When a RTS message is received, the receiver may not respond to it if it senses the medium busy. In this case the CTS is not sent and the sender of the RTS will interpret this as a collision. From the efficiency point of view this is less prejudicial than a real collision, since a single retransmission is required of the ignored RTS. Real collisions, causes the retransmission of both the RTS and the large data frame that was already being transmitted or received by the receiver. The amount of RTS messages ignored by the receiver is represented by the second layer of Fig. 15 in light yellow, and it is higher for Scenario A2.

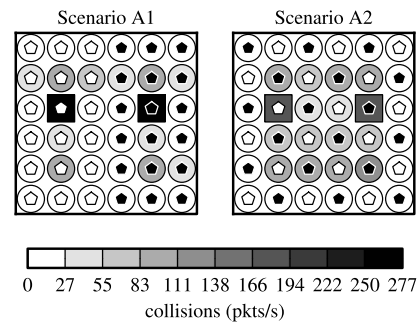


Fig. 16 Amount of collisions on the networks of scenarios of Fig. 11 when each node is generating a flow of 3 Mbit/s to a destination on the Internet. The *white* and *black centers* of each node represent the gateway used to forward the packets to the Internet. The *face color* of a node represents the amount of collisions perceived by that node

If the RTS is not ignored and the medium is free, a CTS message is sent. In our experiences, CTS packets were always successfully delivered. The sender, then transmits the data frame. The number of data frame collisions, represented by the third layer of Fig. 15 in light green, is very low in both scenarios because the RTS/CTS mechanism avoids most of this type of collisions.

The dark blue bottom layer of Fig. 15 represent the per-hop throughput and it confirms the results also presented in Fig. 12(a) showing that Scenario A2 has a higher per-hop throughput than Scenario A1.

Figure 16 shows the amount of collisions for each scenario when each node generates a traffic flow of 3 Mbit/s, that corresponds to the saturation point referred earlier. Data collisions and RTS collisions are now considered on the receiver of each link. This graph shows that despite the gateway nodes of Scenario A1 have experienced more collisions than gateways of Scenario A2, the total number of collisions of Scenario A2 is higher because all the interior nodes of Scenario A2 suffer collisions, while in Scenario A1 only the a third of all nodes suffer collisions.

4.7 Mean hop count

An experiment was performed to understand the impact of the mean hop count on the end-to-end throughput of the networks of Scenario A1 and Scenario A2. Nodes on positions 2, 4, 6, 9, 11, 27, 29, 32, 34 and 36 (refer to Fig. 9) were removed from networks on both scenarios in order to get similar mean hop count; the resulting networks are Scenario B1 and Scenario B2, shown in Fig. 17(a).

The networks of Scenarios B were subjected to the same tests and loads described before. The achieved end-to-end throughputs with the correspondent 90 % confidence intervals and the topology metrics are also shown in Fig. 17. The shape of these graphs are similar to those presented in Fig. 12 showing that the mean hop count of these networks does not have a great impact on the network performance.

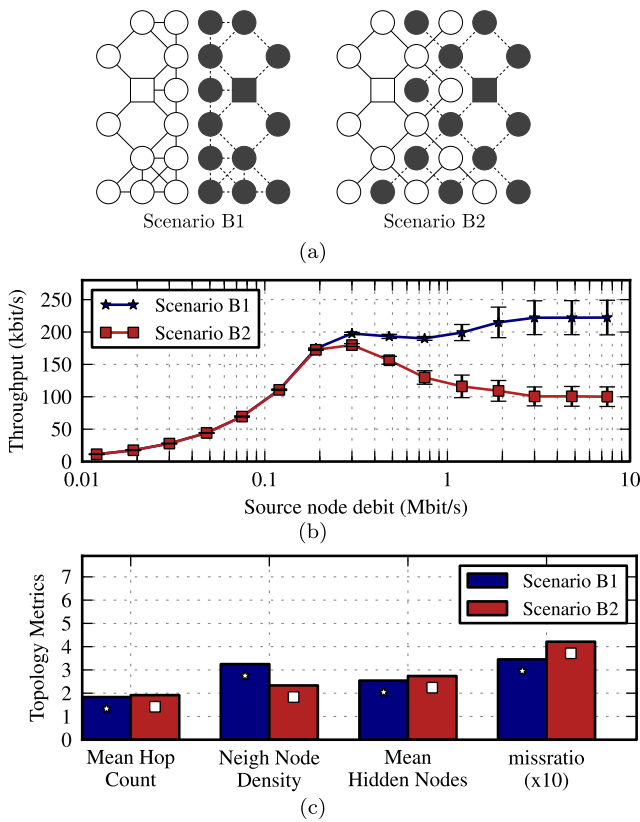


Fig. 17 The network topology, end-to-end throughput with 90 % confidence intervals and topology metrics of a reduced version of scenarios on Fig. 11, where nodes on positions 2, 4, 6, 9, 11, 27, 29, 32, 34 and 36 (refer to Fig. 9) were removed

Table 2 Total end-to-end throughput of the network is higher on Scenarios A1 and A2 than in with B1 and B2

| T_{A1} | T_{A2} | T_{B1} | T_{B2} |
|---------------------------------------|---------------------------------------|---------------------------------------|---------------------------------------|
| $34 \times 170 = 5.78 \text{ Mbit/s}$ | $34 \times 130 = 4.42 \text{ Mbit/s}$ | $24 \times 220 = 5.28 \text{ Mbit/s}$ | $24 \times 180 = 4.32 \text{ Mbit/s}$ |

An increase of about 30 % on the maximum end-to-end throughput was observed for Scenarios B1 and B2, when compared with Scenarios A1 and A2. This increase was expected since fewer nodes are sharing the gateways and the channel. However, the maximum total end-to-end throughput of the network $T = N\lambda_{max}$ is higher on Scenarios A1 and A2 as shown in Table 2.

4.8 Neighbor node density in the single channel scenario

Figure 12(b) shows that the single channel scenario presents an end-to-end throughput higher than the scenarios using two channels. This result is true when the two gateways are deployed beyond the carrier sensing range of each other. The following experiment was performed to understand the impact of increasing the carrier sensing distance on the net-

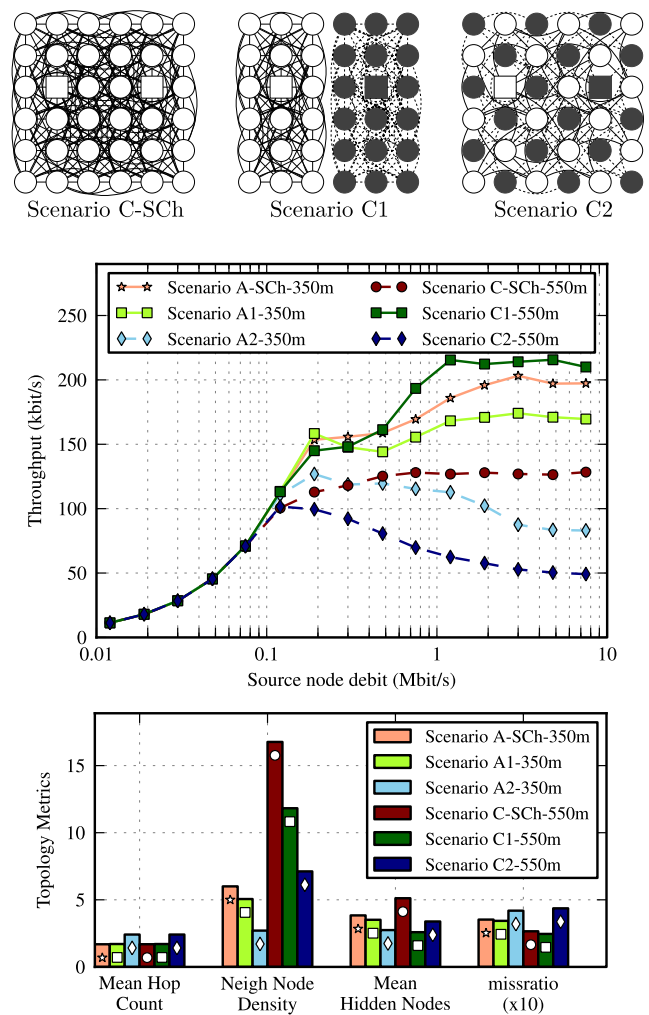


Fig. 18 Network topology when carrier sense range is 550 m using the same channel schemes of Fig. 11. When the carrier sense range enables the gateways to sense each other's transmissions, the single channel scenario (Scenario C-Sch) performance is lower than the Scenario A-Sch. The decrease and increase respectively of hidden nodes from Scenario A1 to Scenario C1 and A2 to C2 justifies the increase and decrease on the end-to-end throughput

work end-to-end throughput. The networks of Fig. 11 were configured with a carrier sensing threshold that guarantees a carrier sensing range of 550 m, which enables gateways to sense each other's transmissions. The resultant networks and their wireless connections are presented in Fig. 18; these networks were subjected to the same tests and loads described before. The achieved end-to-end throughputs and the topology metrics are also shown in Fig. 18; the correspondent confidence intervals were omitted in order to simplify the figure, but they are of the same order of those represented in Fig. 12.

In the Scenario A-Sch (Single Channel) with carrier sensing range configured to 350 m (Fig. 12), the two gateways are on the same channel but not on the communication range of each other, therefore they can receive traffic from

neighboring nodes simultaneously. When the carrier sensing range enables the gateways to sense each other's transmissions, as in Scenario C-Sch of Fig. 18, the gateways share the channel and are on the communication range of each other; it implies that gateways cannot receive packets simultaneously and there is a decrease of network end-to-end throughput as shown by Fig. 18, when comparing Scenario C-Sch and Scenario A-Sch.

Another interesting result is that end-to-end throughput of Scenario C1 is higher than Scenario A1 while Scenario C2 presents lower end-to-end throughputs than Scenario A2, as shown by the end-to-end throughput graph of Fig. 18. This can be explained by the *miss ratio*, the mean number of hidden nodes and the neighbor node density. As shown in the topology metrics graph of Fig. 18, all channel assignment schemes with wider carrier sensing range—Scenarios C1, C2 and C-Sch—have neighbor node densities higher than schemes of Scenarios A1, A2 and A-Sch. However, the number of hidden nodes and the *miss ratio* have different behaviors for the different channel assignment schemes when the neighbor node density increases. When it comes to Scenarios A1 and C1, the mean number of hidden nodes and *miss ratio* decreases when the neighbor node density rises; for Scenarios A2 and C2 as well as single channel scenarios A-Sch and C-Sch, the mean number of hidden nodes and *miss ratio* increases with the neighbor node density.

4.9 Gateways position in the single channel scenario

In order to confirm that single channel scenarios, where gateways are placed on the communication range of each other, present worst results than when two channels are used, a new experiment was carried out. The gateways were deployed in positions 15 and 21 (refer to Fig. 9), as shown in Fig. 19. The networks of Scenarios D were subjected to the same tests and loads described before. The achieved end-to-end throughputs with the correspondent 90 % confidence intervals and the topology metrics are also shown in Fig. 19. The end-to-end throughput for single channel scenario with centered gateways, Scenario D-Sch on Fig. 19, is less than half of the end-to-end throughput obtained when the gateways are out of the communication range of each other (Scenario A-Sch on Fig. 12(b)).

In Scenario D-Sch it is possible to have different routing paths on each simulation run. Different routing paths turns out in different *miss ratios* as shown by the wider confidence interval of *miss ratios* on Scenario D-Sch presented in the topology metrics graph on Fig. 19. These variations on *miss ratio* leads to variations on the end-to-end throughput as shown by the wider confidence intervals of end-to-end throughputs of Scenario D-Sch when compared with Scenario D1 and Scenario D2.

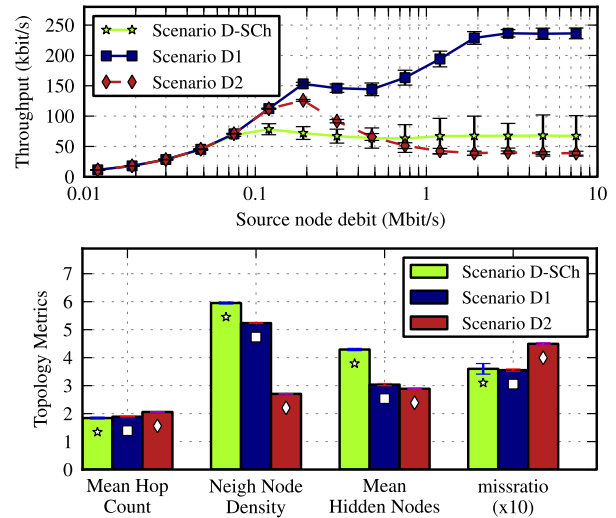
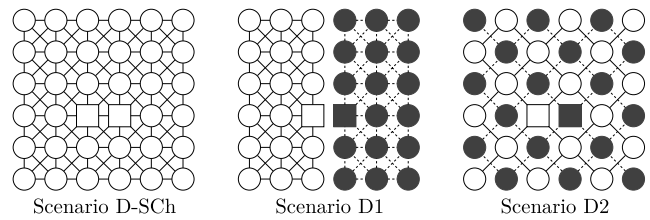


Fig. 19 Network topology, end-to-end throughputs with 90 % confidence intervals and topology metrics when gateways are deployed in positions 15 and 21 on the center of the network

4.10 Size of the gateway neighborhood

In order to understand the impact of the characteristics of a gateway neighborhood, Scenarios E1, E2, E3 and E4 were simulated. These scenarios, on Fig. 20, show channel assignment schemes with 1, 2 and 3 nodes around the gateway. Scenarios E1 and E4 are, respectively, based on Scenarios A2 and A1 presented in Fig. 11, moving the gateways to the corners of the lattice. Scenarios E2 and E3 are variants of Scenario E1 where the gateway neighborhood was modified to get respectively 2 and 3 nodes around the gateway.

The networks of Fig. 20 were offered the same traffic and tests described earlier. The networks end-to-end throughputs with 90 % confidence intervals and the topology metrics are also presented in Fig. 20.

Results in Fig. 20 show that end-to-end throughput depends on the 1st ring size which is the neighbor node density around the gateway. The higher is the 1st ring size, the higher is the end-to-end throughput obtained. Also, the mean hop count and the *miss ratio* shown in the topology metrics graph of Fig. 20 present an inverse relationship with the observed end-to-end throughputs shown in the end-to-end throughputs graph; in this case the higher is the hop count and *miss ratio* the lower are the end-to-end throughputs obtained.

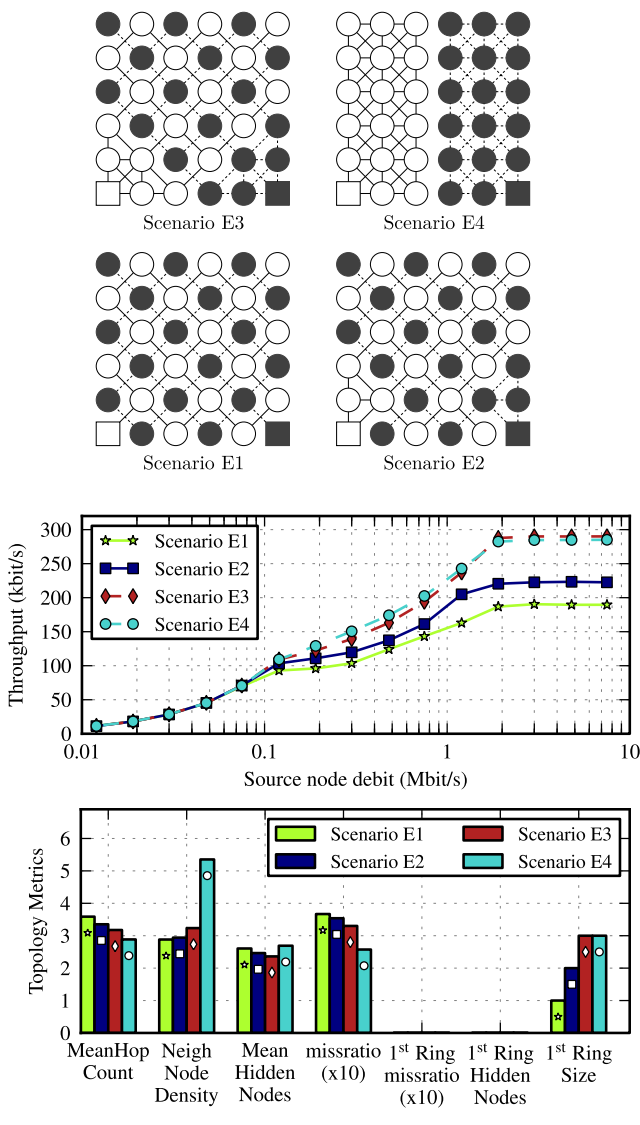


Fig. 20 Channel assignment schemes with few full connected nodes on the neighborhood of the gateway. End-to-end throughputs with 90 % confidence intervals and topology metrics are also presented

The end-to-end throughput obtained in Scenario E3 and Scenario E4 are similar. Curiously, most of these two topologies metrics are different, except the size of the 1st ring. This observation enable us to conclude that the size of the 1st ring may have a great importance on the performance of the network.

From the 4 channel assignment schemes tested, Scenario E3 and Scenario E4 present the highest end-to-end throughput. In fact, the 290 kbit/s achieved is near the maximal theoretical end-to-end throughput for a 34 flows destined to 2 gateways when the channel data rate is 11 Mbit/s, which is 323 kbit/s as explained above. Additional random channel assignment schemes with 34 nodes plus 2 gateways were tested and the maximum observed end-to-end throughput was found always below 300 kbit/s per node. All the

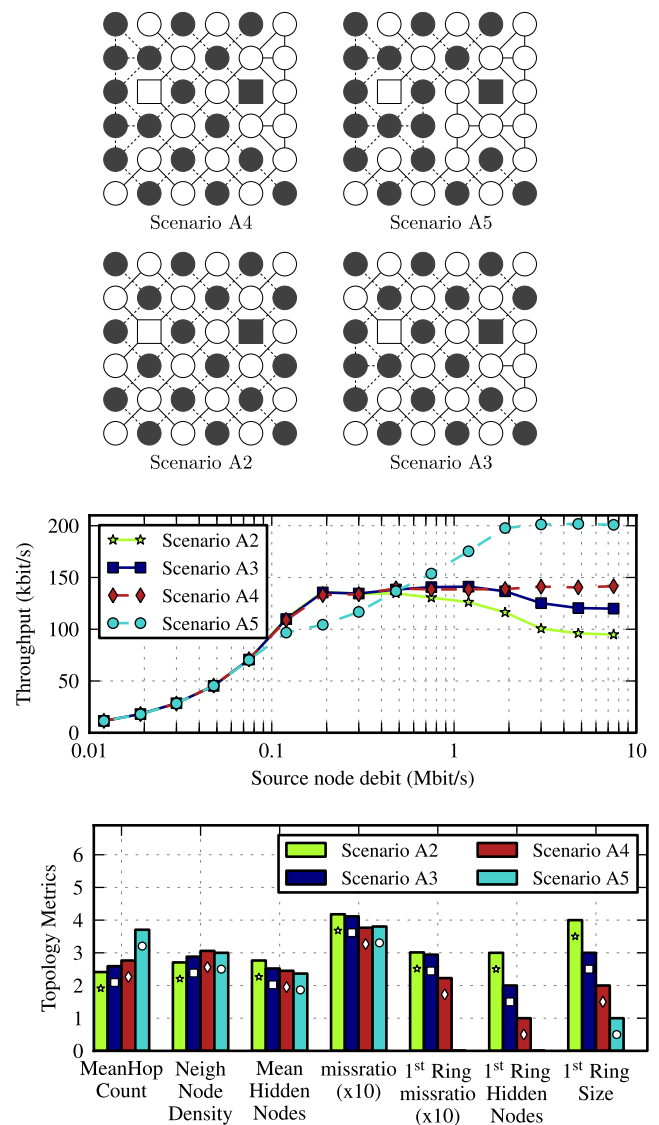


Fig. 21 Channel assignment schemes with few nodes on the neighborhood of the gateway, all hidden from each other. End-to-end throughputs with 90 % confidence intervals and topology metrics are also presented

scenarios reaching near the maximum end-to-end throughput, have similar 1st ring topology characteristics: three full connected nodes around the gateway.

4.11 Hidden nodes on the gateway neighborhood

In order to verify the impact of 1st ring hidden nodes and 1st ring *miss ratio* on the network performance, the scenarios of Fig. 21 were also tested. Scenarios A3, A4 and A5 are variants of Scenario A2, previously presented in Fig. 11, where size of 1st ring becomes respectively 3, 2 and 1. On these scenarios, all 1st ring nodes are hidden from each other in order to verify the importance of 1st ring size in the presence of hidden nodes around the gateway.

The networks on Fig. 21 were offered to the same traffic and tests described earlier. The networks end-to-end throughputs and the topology metrics are also presented in Fig. 21; the correspondent confidence intervals were omitted in order to simplify the figure, but are of the same order as those represented in Fig. 20.

In opposition to what was observed in Fig. 20, for Scenarios A2, A3, A4 and A5 the end-to-end throughput decreases with the increase of the size of the 1st ring size, as shown in Fig. 21. However, on scenarios of Fig. 21, the number of hidden nodes around the gateway increases with the increase of 1st ring size. Based on that, we conclude that the number of hidden nodes on the 1st ring influences more the network performance than the size of the 1st ring.

The $miss\ ratio_{R1}$ is the $miss\ ratio$ calculated considering only the links hidden from 1st ring links, as defined in Sect. 2. The $miss\ ratio_{R1}$ shown in the topology metrics graph of Fig. 21 are clearly related with the end-to-end throughput also shown in that figure. The $miss\ ratio_{R1}$ of Scenarios A2, A3 and A4 have small differences between them, while the $miss\ ratio_{R1}$ of Scenario A5 is much smaller. Notably, this relationships are also present between the end-to-end throughputs of Scenarios A2, A3, A4 and A5 on Fig. 21.

Scenario A5 has the best performance presented in Fig. 21 because it has a single node on the 1st ring and therefore does not have nodes hidden from this single link to the gateway. However, the end-to-end throughput of Scenario A5 does not reach the maximum achievable end-to-end throughput observed at Scenarios E3 and E4 on Fig. 20 because a single link of Scenario A2 is not able to make hay of channel capacity as the three 1st ring links of Scenarios E3 and E4.

Having three nodes on the 1st ring that cannot hear each other, as on Scenario A3, causes a great amount of collisions between them causing inefficiency on the network bottleneck which is the gateway neighborhood. On the contrary, when there are three nodes on the 1st ring that can hear each other, the medium around the gateway is used more efficiently, leading to better network end-to-end throughputs as shown by Fig. 22.

The amount of collisions on Scenarios E4, E3 and A3 are shown on Fig. 22(b). Scenarios E4 and E3 present less collisions around the gateway than Scenario A3. The amount of collisions and consequent network inefficiency is related to the number of hidden nodes on the 1st ring. The inefficiency around the gateway has high impact in the network end-to-end throughput, since it is the network bottleneck.

5 Random scenarios results

In this section we aim to generalize the findings of Sect. 4 analyzing the a set of experiments done with 8000 random

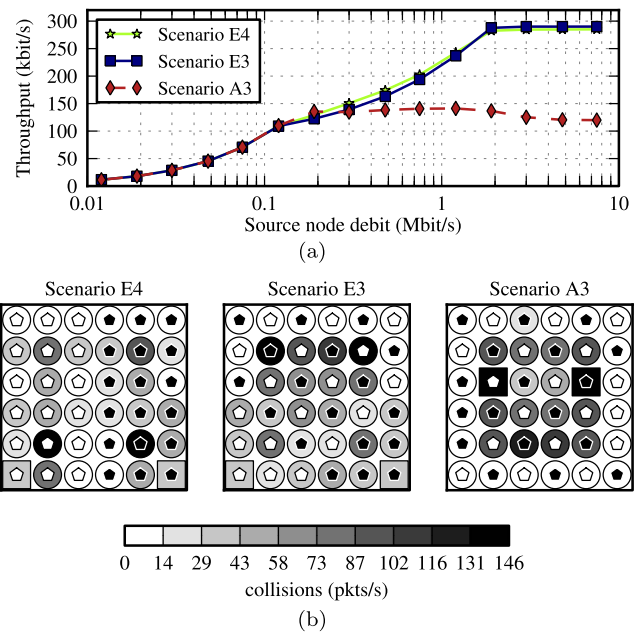


Fig. 22 Comparison of the end-to-end throughputs of networks of Scenarios E4, E3 of Fig. 20 and Scenario A3 of Fig. 21

scenarios. We simulated the scenarios with high traffic load conditions with 3 different seeds as described in Sect. 3. We measured the end-to-end throughput and topology metrics of each of the sub-networks. The five topology metrics introduced earlier were considered: mean hop count, node density, $miss\ ratio$, 1st ring size, and 1st ring $miss\ ratio$. The set of 48000 experiments (8000 topologies \times 3 seeds \times 2 sub-networks) was studied statistically considering that each of the metrics is a random variable and the measures taken from the simulation are samples of those variables. The probability density function (PDF) of each topology metric as well as of the end-to-end throughput is shown in Fig. 23. The mean values of topology metrics are listed on Table 3 and are shown in the graphs of Fig. 23 as a red vertical line. The end-to-end throughput has a mean value 240.7 kbit/s which is of the same order of magnitude of the values obtained for lattice topologies studied on Sect. 4.

In order to evaluate the impact of each topology metrics on the end-to-end throughput we analyzed their joint PDF. Since each topology metric has a large range of values, using all experiments to plot the joint PDF could lead to erroneous conclusions since it would be difficult to isolate the impact of each individual topology metric on the end-to-end throughput. Therefore we used the following methodology to do the sensitivity analysis: a joint PDF of a given topology metric was plotted while fixing the other four topology metrics on the most frequent range of values listed in Table 3. These ranges correspond to the most frequent bin of a histogram of three bins. When four topology metrics are held within a fixed range, only a fraction of the complete set

of 48000 experiments is considered. The number of experiments considered for each joint PDF are listed in Table 3 and vary between 21.2 % and 24.8 % of the 48000 experiments. Narrower ranges conduct to a small number of experiments available to plot the joint PDF.

Figure 24 shows the five joint PDF graphs of a topology metric and the end-to-end throughput. To ease the reading of the joint PDF, the correspondent simple PDF of each topology is shown on the top of the joint PDF and the simple PDF of the end-to-end throughput is shown on the right side of Fig. 24. Note that the sample space size (range of values) of each of the topology metrics was slightly reduced due to sensitivity analysis methodology while the end-to-end throughput sample space size was kept the same. The x axes of each joint PDF graph represent the correspondent topology metric. The y axis of all joint PDF graphs refer to the end-to-end throughput presenting the same range. On the joint PDF graphs, darker spots represent more frequent occurrences of experiments with a x topology metric and a y throughput. The linear correlation ρ between the end-to-end throughput and each of the topology metrics, presented in the graphs of Fig. 24 and in Table 3, is given by Eq. (10), where \bar{x} and σ_x are respectively the mean value and standard deviation of each of the topology metrics samples, \bar{y} and σ_y are respectively the mean value and standard deviation of

end-to-end throughput of the samples, and n_e is the number of considered experiments; ρ can take values in the interval $[-1, 1]$, where $\rho = 0$ means that the throughput and the topology metric are uncorrelated and $|\rho| = 1$ means that the throughput and the topology metric have a linear relation positive ($\rho = 1$) or negative ($\rho = -1$).

$$\rho = \frac{\sum_{i=1}^{n_s} (x_i - \bar{x})(y_i - \bar{y})}{(n_e - 1)\sigma_x\sigma_y} \tag{10}$$

The 1st ring *miss ratio* has the highest impact on end-to-end throughput ($|\rho| = 0.76$). The joint PDF shown on Fig. 24(e) reveals a strong relation between these metrics because most of the spots are located on the vicinity of a straight line with a negative slope. This strong relation is confirmed by the correlation value of -0.76 which has the highest absolute value observed. We can observe that high values of end-to-end throughput only exist when the 1st ring *miss ratio* is low.

The graph on Fig. 24(d) also has most of the spots on the vicinity of a straight line but with positive slope, showing that 1st size and the end-to-end throughput are positively correlated; this result is confirmed by the correlation value of 0.55 obtained. We can observe that high values of end-to-end throughput only exist when the 1st size is high.

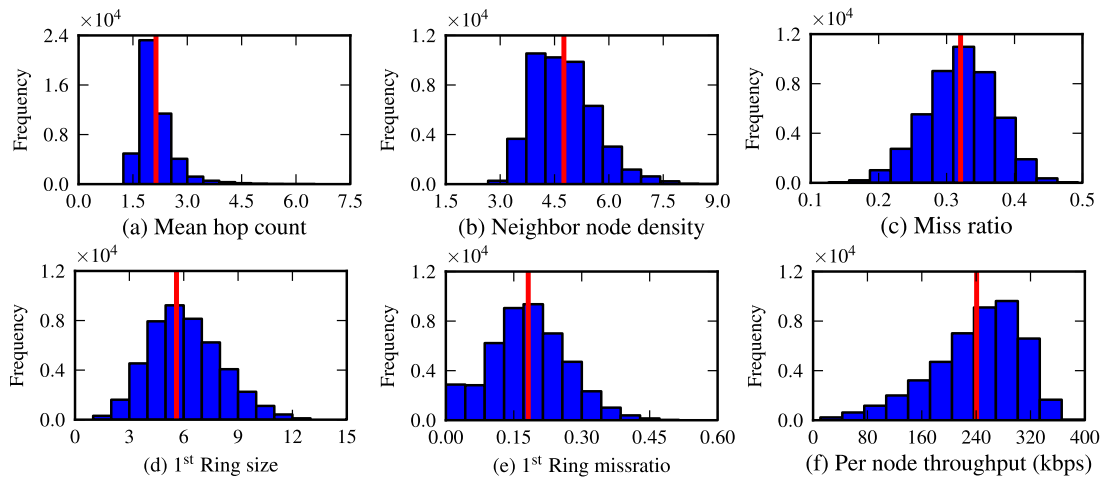


Fig. 23 Histograms of end-to-end throughput and topology metrics of the 8000 random scenarios simulated

Table 3 Values of correlation ρ between end-to-end throughput and topology metrics

| | Mean hop count | Node density | <i>miss ratio</i> | Size of 1st ring | 1st ring <i>miss ratio</i> |
|---------------------|----------------|--------------|-------------------|------------------|----------------------------|
| Mean | 2.14 | 4.76 | 0.32 | 5.6 | 0.18 |
| Range most frequent | [1.24, 3.0] | [2.67, 4.8] | [0.25, 0.37] | [5, 9] | [0.17, 0.34] |
| No. of experiments | 21.7 % | 24.8 % | 22.2 % | 21.2 % | 23.9 % |
| ρ | -0.141 | -0.013 | -0.369 | 0.549 | -0.762 |

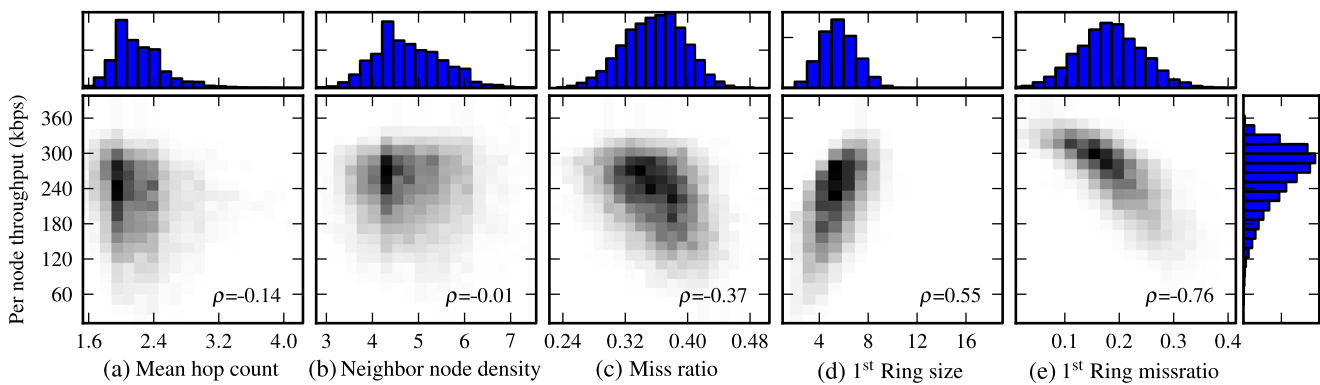


Fig. 24 Joint PDF graphs of end-to-end throughput and five topology metrics: mean hop count, node density, *miss ratio*, 1st ring size, and 1st ring *miss ratio*

The relation between the *miss ratio* and the end-to-end throughput is also relevant, as shown by their correlation value of -0.37 . In this case, the spots on joint PDF graph (Fig. 24(c)) are more spread but a darker area can be observed around a line with a negative slope. We can observe that high values of end-to-end throughput only exist when the *miss ratio* is not very high.

A tenuous relation between the mean hop count end-to-end throughput is shown by the joint PDF graph of Fig. 24(a). The -0.14 correlation between these two metrics show that a light relation can exist. We can observe that high values of end-to-end throughput are more frequent when the mean hop count is low.

The joint PDF graph of Fig. 24(b) do not show any relation between the neighbor node density and the end-to-end throughput. The correlation of -0.01 confirms this lack of relation between these two metrics. We can infer that there are no relation between the neighbor node density end-to-end throughput.

6 Conclusions

Using Stub WMNs based in IEEE 802.11 to extend Internet access requires strategies to improve the network performance such as the use of multiple channels. When a single radio is available on each channel to form the WMN, the use of multiple channels results on the creation of multiple subnetworks, one per channel. The topology characteristics of these subnetworks affect the network performance but can be controlled by the channel assignment to nodes. In this paper we clarify which topology characteristics are relevant to improve performance and which metrics can be used to measure them.

Topology metrics related with hop count, neighbor node density, and hidden nodes were identified and studied with emphasis on how such metrics have been treated in previous works on wireless networks. These topology characteristics

and metrics are treated separately in the literature. In this work, we address them jointly.

Extensive simulations using ns-2 were performed to evaluate the impact of topology characteristics on the throughput of single-radio WMN. The analysis of arbitrary channel assignment schemes to a 36 node lattice gave important hints about the relative importance of network topology characteristics in network performance. A statistical analysis of simulation of a set of 8000 random 36 node networks scenarios confirmed that the findings discovered by the study on the arbitrary lattice topologies are true for a general network topologies, namely:

1. the number of hidden nodes on the gateway neighborhood and the number of nodes around the gateway have a huge impact on the network performance, since the gateway neighborhood is the network bottleneck and it is important to use it efficiently;
2. the effects of hidden nodes measured by *miss ratio* can be a significant metric when predicting the performance of a given topology;
3. mean hop count and neighbor node density have low impact on the network performance for the topologies studied in this paper.

Since fairness is an important metric when characterizing the performance of a WMN, it should be addressed in future work. We believe that the knowledge obtained with this study can be applied to the efficient planning of single radio mesh networks based on CSMA/CA.

Acknowledgements This work was co-supported by the SitMe project from QREN-ON.2 program, the MC-WMNs project (PTDC EEA TEL 120176/2010) from Fundação para a Ciencia e Tecnologia (FCT), and the FCT grant SFRH BD S13444/2003.

References

1. Abdullah, A., Gebali, F., & Cai, L. (2009). Modeling the throughput and delay in wireless multihop ad hoc networks. In

- IEEE Global Telecommunications Conf. (GLOBECOM'09)*, USA (pp. 1–6).
2. Adya, A., Bahl, P., Padhye, J., Wolman, A., & Zhou, L. (2004). A multi-radio unification protocol for IEEE 802.11 wireless networks. In *Proc. inter. conf. on Broadband Networks (BroadNets'04)* (pp. 344–354). New York: IEEE Press.
 3. Alicherry, M., Bhatia, R., & Li, L. E. (2005). Joint channel assignment and routing for throughput optimization in multi-radio wireless mesh networks. In *Proc. inter. conf. on mobile computing and networking (MobiCom'05)*, Germany (pp. 58–72). doi:10.1145/1080829.1080836.
 4. Ashraf, U., Abdellatif, S., & Juanole, G. (2011). Route selection in IEEE 802.11 wireless mesh networks. *Telecommunications Systems*. doi:10.1007/s11235-011-9493-5.
 5. Avallone, S., D'Elia, F. P., & Ventre, G. (2011). A new channel, power and rate assignment algorithm for multi-radio wireless mesh networks. *Telecommunications Systems*. doi:10.1007/s11235-010-9416-x.
 6. Bachir, A., Barthel, D., Heusse, M., & Duda, A. (2005). Hidden nodes avoidance in wireless sensor networks. In *Proc. inter. conf. wireless networks, communications and mobile computing (WirelessCom'05)*, USA (Vol. 1, pp. 612–617). doi:10.1109/WIRELES.2005.1549478.
 7. Bahl, P., Chandra, R., & Dunagan, J. (2004). SSCH: slotted seeded channel hopping for capacity improvement in IEEE 802.11 ad hoc wireless networks. In *Proc. inter. conf. on mobile computing and networking (MobiCom'04)*, USA (pp. 216–230). doi:10.1145/1023720.1023742.
 8. Calçada, T., & Ricardo, M. (2011). The impact of network topology on the performance of multi-channel single-radio mesh networks. In *Proc. of networking and electronic commerce rsrch. conf (NAEC'11)*, Italy.
 9. Chan, C. P., Liew, S. C., & Chan, A. (2009). Many-to-one throughput capacity of IEEE 802.11 multihop wireless networks. *IEEE Transactions on Mobile Computing*, 8(4), 514–527. doi:10.1109/TMC.2008.130.
 10. Crichigno, J., Wu, M., & Shu, W. (2008). Protocols and architectures for channel assignment in wireless mesh networks. *Ad Hoc Networks*, 6(7), 1051–1077. doi:10.1016/j.adhoc.2007.10.002.
 11. Dhananjay, A., Zhang, H., Li, J., & Subramanian, L. (2009). Practical, distributed channel assignment and routing in dual-radio mesh networks. *Computer Communication Review*, 39(4), 99–110.
 12. Gupta, P., & Kumar, P. R. (2000). The capacity of wireless networks. *IEEE Transactions on Information Theory*, 46(2), 388–404.
 13. IEEE802.11 IEEE wireless LAN medium access control (MAC) and physical layer (PHY) specifications (2007).
 14. IEEE802.11s IEEE wireless LAN medium access control (MAC) and physical layer (PHY) specifications draft on mesh networking (2009).
 15. Jiang, L. B., & Liew, S. C. (2008). Improving throughput and fairness by reducing exposed and hidden nodes in 802.11 networks. *IEEE Transactions on Mobile Computing*, 7(1), 34–49. doi:10.1109/TMC.2007.1070.
 16. Jun, J., Peddabachagari, P., & Sichitiu, M. (2003). Theoretical maximum throughput of IEEE 802.11 and its applications. In *Proc. inter. symp. network computing and applications (NCA'03)*, USA, pp. 249–256. doi:10.1109/NCA.2003.1201163.
 17. Jun, J., & Sichitiu, M. (2003). The nominal capacity of wireless mesh networks. *IEEE Wireless Communications*, 10(5), 8–14.
 18. Jun, J., & Sichitiu, M. (2004). Fairness and QoS in multihop wireless networks. In *IEEE vehicular technology conf. (VTC-Fall'03)* (pp. 2936–2940).
 19. Kodialam, M., & Nandagopal, T. (2005). Characterizing the capacity region in multi-radio multi-channel wireless mesh networks. In *Proc. inter. conf. on mobile computing and networking (MobiCom'05)*, Germany (pp. 73–87).
 20. Kuo, J., Liao, W., & Hou, T. (2009). Impact of node density on throughput and delay scaling in multi-hop wireless networks. *IEEE Transactions on Wireless Communications*, 8(10), 5103–5111. doi:10.1109/TWC.2009.071467.
 21. Kyasanur, P., & Vaidya, N. H. (2005). Capacity of multi-channel wireless networks: impact of number of channels and interfaces. In *Proc. inter. conf. on mobile computing and networking (MobiCom'05)*, Germany (pp. 43–57). doi:10.1145/1080829.1080835.
 22. Li, J., Blake, C., Couto, D. S. D., Lee, H. I., & Morris, R. (2001). Capacity of ad hoc wireless networks. In *Proc. inter. conf. on mobile computing and networking (MobiCom'01)*, Italy (pp. 61–69). doi:10.1145/381677.381684.
 23. Marina, M. K., Das, S. R., & Subramanian, A. P. (2010). A topology control approach for utilizing multiple channels in multi-radio wireless mesh networks. *Computer Networks*, 54(2), 241–256.
 24. Matos, R., Sargento, S., Hummel, K. A., Hess, A., Tutschku, K., & Meer, H. (2011). Context-based wireless mesh networks: a case for network virtualization. *Telecommunications Systems*. doi:10.1007/s11235-011-9434-3.
 25. Nagesh, S. N., Deepti, S. N., Cavalcanti, D., & Agrawal, D. P. (2006). A novel queue management mechanism for improving performance of multihop flows in IEEE 802.11 s based mesh networks. In *Proc. inter. conf. performance, computing, and communications (IPCCC'06)*, USA, pp. 162–168. doi:10.1109/2006.1629403.
 26. Ng, P. C., & Liew, S. C. (2007). Throughput analysis of IEEE802.11 multi-hop ad hoc networks. *IEEE/ACM Transactions on Networking*, 15(2), 309–322.
 27. Ramachandran, K., Sheriff, I., Belding, E., & Almeroth, K. (2008). A multi-radio 802.11 mesh network architecture. *Mobile Networks and Applications*, 13(1), 132–146. doi:10.1007/s11036-008-0026-8.
 28. Robinson, J., Papagiannaki, K., Diot, C., Guo, X., & Krishnamurthy, L. (2005). Experimenting with a Multi-radio mesh networking testbed. In *Proc. inter. wksp. on wireless network measurements (WINMEE'05)*, Italy. doi:10.1.1.115.4729.
 29. Skalli, H., Ghosh, S., Das, S., Lenzini, L., & Conti, M. (2007). Channel assignment strategies for multiradio wireless mesh networks: issues and solutions. *IEEE Communications Magazine*, 45(11), 86–95. doi:10.1109/MCOM.2007.4378326.
 30. So, J., & Vaidya, N. (2006). Load-balancing routing in multichannel hybrid wireless networks with single network interface. *IEEE Transactions on Vehicular Technology*, 55(3), 806–812. doi:10.1109/TVT.2006.874550.
 31. So, J., & Vaidya, N. H. (2004). Multi-channel mac for ad hoc networks: handling multi-channel hidden terminals using a single transceiver. In *Proc. inter. symp. on mobile ad hoc networking and computing (MobiHoc'04)*, Japan (pp. 222–233).
 32. Subramanian, A., Gupta, H., Das, S., & Cao, J. (2008). Minimum interference channel assignment in multiradio wireless mesh networks. *IEEE Transactions on Mobile Computing*, 7(12), 1459–1473.
 33. Vedantham, R., Kakumanu, S., Lakshmanan, S., & Sivakumar, R. (2006). Component based channel assignment in single radio, multi-channel ad hoc networks. In *Proc. inter. conf. on mobile computing and networking (MobiCom'06)*, USA (pp. 378–389). doi:10.1145/1161089.1161132.
 34. Wang, B., Lim, H. B., Ma, D., & Fu, C. (2010). The hop count shift problem and its impacts on protocol design in wireless ad hoc networks. *Telecommunications Systems*, 44(1–2), 49–60. doi:10.1007/s11235-009-9221-6.
 35. Xu, K., Gerla, M., & Bae, S. (2002). How effective is the IEEE 802.11 RTS/CTS handshake in ad hoc networks. In *Proc. IEEE global telecom. conf (GLOBECOM'02)*, Taiwan (Vol. 1, pp. 72–76).

36. Yang, J., Kwon, J., Hwang, H., & Sung, D. (2009). Goodput analysis of a WLAN with hidden nodes under a non-saturated condition. *IEEE Transactions on Wireless Communications*, 8(5), 2259–2264. doi:[10.1109/TWC.2009.080632](https://doi.org/10.1109/TWC.2009.080632).



Tânia Calçada received a Licenciatura (1999) degree in Electrical and Computer Engineering from Porto University. Previously she was working for a telecom operator designing corporate network solutions. Currently, she is a researcher at INESC TEC in the area of wireless networks involved in projects related with WMNs and vehicular networks. She is a PhD student on the topic of channel assignment strategies for WMNs.



Manuel Ricardo received a Licenciatura (1988), M.Sc. (1992), and Ph.D. (2000) degrees in Electrical and Computer Engineering from Porto University. Currently, he is an associate professor at the Faculty of Engineering, Porto University, where he gives courses in mobile communications and computer networks. He also coordinates Telecommunications and Multimedia Unit of INESC TEC (<http://www.inescporto.pt/>).